Available on the CERN CDS information server **CMS PAS HIG-12-020**

CMS Physics Analysis Summary

Contact: cms-pag-conveners-higgs@cern.ch 2012/07/09

Observation of a new boson with a mass near 125 GeV

The CMS Collaboration

Abstract

Combined results are presented from searches for the standard model (SM) Higgs boson in proton-proton collisions at $\sqrt{s} = 7$ and 8 TeV in five decay modes: $\gamma\gamma$, bb, $\tau\tau$, WW, and ZZ. The analysed data correspond to integrated luminosities of up to 5.1 fb^{-1} at 7 TeV and 5.3 fb^{-1} at 8 TeV. The data exclude the existence of a SM Higgs boson in the ranges 110–122.5 and 127–600 GeV at 95% confidence level. An excess of events above the expected SM background is observed with a local significance of 4.9σ around 125 GeV, which we attribute to the production of a previously unobserved particle. The evidence is strongest in the two final states with the best mass resolution: the two-photon final state and the final state with two pairs of charged leptons (electrons or muons). The combined excess in these channels alone gives a local significance of 5.0σ. An unconstrained fit to the excesses in these two final states yields a mass of 125.3 $\pm$ 0.4 (stat) $\pm$ 0.5 (syst) GeV. Within the statistical uncertainties, the results obtained in all search channels are consistent with the expectations for a SM Higgs boson. More data are needed to test whether the properties of this new state are indeed those of the SM Higgs boson or whether some differ, implying new physics beyond the standard model.

1 Introduction

The discovery of the mechanism for electroweak symmetry breaking is one of the goals of the physics programme at the Large Hadron Collider (LHC). In the standard model (SM) [1–3], this symmetry breaking is achieved by introducing a complex scalar doublet, leading to the prediction of the Higgs boson (H) [4–9]. Precision electroweak measurements indirectly constrain the SM Higgs boson mass m_{H} to be less than 152 GeV [10]. To date, direct experimental searches for this particle have restricted the allowed mass range to 116.6–119.4 GeV and 122.1–127.5 GeV at 95% CL [11–17].

We have previously reported the observation of an excess of events above the expected SM background in the mass region near 125 GeV [CMScombFeb2012, CMScombMar2012]. We also stated that more data are required to ascertain the origin of the observed excess. In this note, we report on the combination of the results from the searches for the Higgs boson carried out in proton-proton collisions at $\sqrt{s} = 7$ and 8 TeV using the Compact Muon Solenoid (CMS) detector [18] at the LHC. The analysed data recorded in 7 TeV collisions (2010-2011 run) and 8 TeV collisions (2012 run) correspond to an integrated luminosity of 4.9–5.1 fb^{-1} and 5.1–5.3 fb^{-1}, respectively. The integrated luminosity ranges reflect the small differences in the amount of data used by the different search channels. The search is performed for Higgs boson masses in the range 110–600 GeV (finding a significant excess above 130 GeV would imply a signal not compatible with the SM Higgs boson that is already excluded in the mass range 130–600 GeV [16, 17]).

The CMS apparatus consists of a barrel assembly and two endcaps, comprising, in successive layers outwards from the collision region, the silicon pixel and strip tracker, the lead tungstate crystal electromagnetic calorimeter, the brass/scintillator hadron calorimeter, the superconducting solenoid, and gas-ionization chambers embedded in the steel return yoke for the detection of muons.

Early phenomenological work on Higgs boson production and decay can be found in Refs. [19–25]. There are four main mechanisms for Higgs boson production in pp collisions at $\sqrt{s} = 7 - 8$ TeV. The gluon-gluon fusion mechanism has the largest cross section, followed in turn by vector boson fusion (VBF), associated WH and ZH production, and production in association with top quarks, $\mathrm{t\bar{t}H}$. The cross sections for the Higgs boson production mechanisms and the decay branching fractions, together with their uncertainties, are taken from Refs. [26–28] and are derived from Refs. [29–72]. The total cross section at $\sqrt{s}$ =7 (8) TeV varies from 23 (29) to 0.4 (0.6) pb in the explored Higgs boson mass range of 110-600 GeV.

The relevant decay modes of the SM Higgs boson depend strongly on its mass m_{H}. The results presented here are based on the following five decay modes: $\mathrm{H} \to \gamma\gamma$, $\mathrm{H} \to \tau\tau$, followed by leptonic and hadronic decays of τ-leptons, $\mathrm{H} \to \mathrm{bb}$, $\mathrm{H} \to \mathrm{WW}$, followed by $\mathrm{WW} \to \ell\nu\ell\nu$ and $\ell\nu\mathrm{qq}$ decays, and $\mathrm{H} \to \mathrm{ZZ}$, followed by ZZ decays to 4ℓ, $2\ell 2\nu$, $2\ell 2\mathrm{q}$, and $2\ell 2\tau$. Here and throughout, ℓ stands for electrons or muons and q for quarks. For simplicity, $\mathrm{H} \to \tau^+\tau^-$ is denoted as $\mathrm{H} \to \tau\tau$, $\mathrm{H} \to \mathrm{b\bar{b}}$ as $\mathrm{H} \to \mathrm{bb}$, etc. The WW and ZZ decay modes are used over the entire explored mass range. The $\gamma\gamma$, $\tau\tau$, and bb decay modes are used only for $m_{\mathrm{H}} < 150$ GeV since their expected sensitivities are not significant compared to WW and ZZ for higher Higgs boson masses.

For a given hypothesis for the Higgs boson mass, the sensitivity of the search depends on the production cross section of the Higgs boson, its decay branching fraction into the chosen final state, the signal selection efficiency, the mass resolution, and the level of standard model backgrounds in the same or a similar final state. For low values of the Higgs boson mass, the

$H \to \gamma\gamma$ and $H \to ZZ \to 4\ell$ channels play a special role due to the excellent mass resolution for the reconstructed diphoton and four-lepton final states, respectively. The $H \to WW \to \ell\nu\ell\nu$ channel provides high sensitivity but has relatively poor mass resolution due to the presence of neutrinos in the final state. The sensitivity in the bb and $\tau\tau$ decay modes is reduced due to the presence of large background and a poor mass resolution. In the high mass range, the search sensitivity is dominated by the WW and ZZ modes.

Most analyses used in this combination have been re-optimized in order to incorporate improvements in event reconstruction and event selection, and to mitigate the effects due to higher intensity running of the LHC in 2012. All selection criteria in the analyses of the 2011 and 2012 data were fixed before looking at the result in the signal region.

2 Search channels

The results presented in this note are obtained by combining the results from the searches for the Higgs boson exploiting different production and decay modes. A summary of all analyses used in the combination is presented in Table 1 where we list their main characteristics, namely: exclusive final states, the mass range of the search, the integrated luminosity used, and the approximate instrumental mass resolution. The presence of a signal or an upward fluctuation of the background in one of the channels, at a certain value of the Higgs boson mass, is expected to manifest itself as an excess extending around that value for a range corresponding to the m_H resolution.

Table 2 shows modes used in the searches in the not-yet-excluded range of Higgs boson masses ($115 < m_H < 130\,\text{GeV}$). The search modes are grouped in this table by the production and decay modes specifically targeted by the corresponding analyses. The naming convention reflects the signature targeted. None of these signatures is 100% pure.

As an illustration of the search sensitivity of the different channels, Fig. 1 shows the median expected 95% CL upper limit on the ratio of the signal cross section, σ, and the predicted SM Higgs boson cross section, $\sigma_{SM\,H}$, as a function of the SM Higgs boson mass hypothesis. A channel showing values below unity (red horizontal line) would be expected to be able to exclude a Higgs boson of that mass at 95% CL. Fig. 2 shows the expected sensitivities for the observation of the SM Higgs boson in terms of p-values and significances. The methods used for deriving limits and p-values are described in Section 3.

2.1 $H \to \gamma\gamma$

The $H \to \gamma\gamma$ analysis [73] is focused on a search for a narrow peak in the diphoton mass distribution. The event sample is split into two mutually exclusive sets: (i) diphoton events with one forward and one backward jet, consistent with the VBF topology, and (ii) all remaining events. This division is motivated by the consideration that there is a better signal-to-background ratio in the first set compared to the second. For the 8 TeV data, the dijet set of events is split into two classes: events with low and high dijet mass m_{jj}. The non-dijet set, containing over 99% of the data, is subdivided into four classes based on the output of a multivariate discriminant that assigns a high score to signal-like events, based on (i) an event-by-event estimate of the diphoton mass resolution, (ii) a photon identification score for each photon, and (iii) kinematic information about the photons and the diphoton system. The photon identification score is obtained from a multivariate analysis (MVA) discriminant that uses shower shape information and isolation variables to separate prompt photons from those arising from jets. The background in the signal region is estimated from a fit to the observed diphoton mass distribution in data.

2.2 $H \to bb$

The $H \to bb$ search [74] concentrates on Higgs boson production in association with a W or Z boson, in which the focus is on the following decay modes: $W \to e\nu/\mu\nu$ and $Z \to ee/\mu\mu/\nu\nu$. The $Z \to \nu\nu$ decay is identified by requiring large missing transverse energy E_T^{miss}, defined as the modulus of the vector $\vec{E}_T^{miss}$ computed as the negative of the vector sum of the transverse momenta of all reconstructed objects in the detector (leptons, photons, and charged/neutral hadrons) which are not found to arise from additional interactions. The Higgs boson candidate is reconstructed by requiring two b-tagged jets [88] and the search is divided into events where the vector bosons have medium or large transverse momentum and recoil away from the candidate Higgs boson. Events with higher transverse momentum bosons have smaller backgrounds and a better dijet mass resolution. A multivariate analysis technique, trained on simulated signal and background events for several different values of the Higgs boson mass, is used to separate signal and background events. The rates of the main backgrounds, consisting of $W/Z +$ jets and top-quark events, are derived from signal-depleted control samples in data. The WZ and ZZ backgrounds with a Z boson decaying to a pair of b-quarks, as well as the single-top background, are estimated from simulation. The MVA output distribution is used as the final discriminant in the limit setting.

The search for $H \to bb$ is also performed using events where the Higgs boson is produced in association with a top-quark pair [75]. This analysis uses events where the top-quark pair decays to either the lepton-plus-jets ($t\bar{t} \to \ell\nu jjbb$) or dilepton ($t\bar{t} \to \ell\nu\ell\nu bb$) final state. The major background in this search is top-pair production accompanied by extra jets. We use artificial neural networks to discriminate between background and signal events. The rates of background processes are estimated from theoretical expectations, and are further constrained in-situ through the inclusion of background enriched samples in the extraction of the final limit.

2.3 $H \to \tau\tau$

The $H \to \tau\tau$ search [76] is performed using the final-state signatures $e\mu$, $\mu\mu$, $e\tau_h$, $\mu\tau_h$, where electrons and muons arise from leptonic τ-decays and τ_h denotes hadronic τ-decays. Each of these categories is further divided into three exclusive sub-categories based on the number and the type of the jets in the event: (i) events with one forward and one backward jet, consistent with the VBF topology, (ii) events with just one jet, and (iii) events with either no jets or with one jet with a small E_T. The last two categories are further divided by the transverse momentum of the visible tau decay. In each of these categories, we search for a broad excess in the reconstructed $\tau\tau$ mass distribution. The main irreducible background, $Z \to \tau\tau$ production, and the largest reducible backgrounds ($W +$ jets, multijet production, $Z \to ee$) are evaluated from various control samples in data.

The search for $H \to \tau\tau$ decays produced in association with a W or Z boson is conducted in events with three or four leptons in the final state [77, 78]. The WH analysis selects events which have two like-signed electrons or muons and a hadronically-decaying tau: $e^+e^+\tau_h^-$ and $\mu^+\mu^+\tau_h^-$. The ZH analysis is performed in events with an identified $Z \to ee$ or $Z \to \mu\mu$ decay and a Higgs boson candidate with one of the following final states: $e\mu$, $e\tau_h$, $\mu\tau_h$, or $\tau_h\tau_h$. The main irreducible backgrounds to the WH and ZH searches are WZ and ZZ diboson events, respectively. The irreducible backgrounds are estimated using simulation, corrected by control samples in data. The reducible backgrounds in both analyses are W, Z, and $t\bar{t}$ events with at least one quark or gluon jet misidentified as an isolated e, μ, or τ_h. These backgrounds are estimated solely from data by measuring the probability for jets to be misidentified as isolated leptons in background-enriched control regions, and weighting the selected events which fail

the lepton requirements by the misidentification probability.

2.4 $H \to WW$

The $H \to WW^{(*)} \to 2\ell 2\nu$ analysis [81, 82] searches for an excess of events with two leptons of opposite charge, large E_T^{miss}, and up to two jets. Events are divided into six categories, with different background compositions and signal-to-background ratios. For events with no jets, the main background stems from non-resonant WW production; for events with one jet, the dominant backgrounds are from WW and top-quark production. The events are split into same-flavour and different-flavour dilepton sub-channels, since the background from Drell–Yan production is much larger for the same-flavour dilepton events. The two-jet category is optimized to take advantage of the VBF Higgs boson production signature. The main background in this channel is from top-quark production. In the 7 TeV analysis, the same-flavour and different-flavour categories with 2 jets are merged into one. To improve the separation of signal from backgrounds in the 7 TeV analysis, MVA classifiers are trained for a number of Higgs boson masses, and a search is made for an excess of events in the output distributions of the classifiers. The current 8 TeV analysis does not yet use the MVA-based discrimination. All background rates, except for very small contributions from WZ, ZZ, and $W\gamma$, are evaluated from data.

The $H \to WW \to \ell\nu 2q$ analysis [79, 80] searches for an excess of events with one lepton (e or μ), E_T^{miss}, and two or three jets. Events are divided into four categories: (e or μ)$\bigotimes$(2 or 3 jets). In all cases, the dominant background is W + jets. Because of the limited MC statistics for this background, a data-driven method is employed that models W + jets in the signal region from the dijet invariant mass sidebands. Smaller backgrounds include $t\bar{t}$, single top, diboson production (irreducible), and Z + jets, which are modeled from MC, and multijet production (electron channels only) which is estimated from data. Because only one neutrino is produced in this channel, both W bosons can be fully reconstructed, and a four-body mass peak for WW and WZ can be seen. A kinematic fit in which the lepton-missing-transverse-energy system is constrained to the on-shell W mass is performed to improve the resolution and reduce the background. To improve further the separation of signal from backgrounds, MVA classifiers that include the Higgs boson decay angles, the four-body rapidity and the p_T are built separately for each simulated Higgs mass point, for each of the four channels. Events passing an optimized cut on the MVA output are retained and a search is made for an excess of events in the four-body invariant mass distributions.

The $WH \to WWW \to 3\ell 3\nu$ analysis [83] searches for an excess of events with three leptons, electrons or muons, large missing transverse energy, and low hadronic activity. The dominant background is from $WZ \to 3\ell\nu$ production, which is largely reduced by requiring that all same-flavour oppositely charged lepton pairs have a dilepton mass away from m_Z. In addition, oppositely charged leptons are required not to be back-to-back. The background processes with jets misidentified as leptons, e.g. Z + jets and top, as well as the $WZ \to 3\ell\nu$ background are estimated from data. The small contribution from the $ZZ \to 4\ell$ process with one unreconstructed lepton is estimated using simulated samples.

The search for $H \to WW \to 2\ell 2\nu$ events produced in association with a W or Z boson decaying to two jets [84] is performed by selecting events with two oppositely charged leptons, large missing transverse energy and two jets with an invariant mass around the W/Z pole. The main backgrounds that contaminate the signal region are top-quark and Z + jets production and are normalised with data-based techniques, as well as contributions from W + jets and multijet processes, where one or more jets are misidentified as leptons. The WW + jets production is

estimated with simulated events.

2.5 $H \to ZZ$

In the $H \to ZZ^{(*)} \to 4\ell$ channel [85], we search for a four-lepton mass peak over a small continuum background. To further separate signal and background, we use a discriminant calculated for each event as the ratio of the probabilities for signal and background to form an event with the observed kinematics (the masses of the dilepton pairs and the five angles fully defining a four-lepton configuration in their center-of-mass frame). The 4e, 4μ and $2e2\mu$ sub-channels are analysed separately since there are differences in the four-lepton mass resolutions and the background rates arising from jets misidentified as leptons. The dominant irreducible background in this channel is from non-resonant ZZ production with both Z bosons decaying to either 2e, 2μ, or 2τ (with the taus decaying leptonically) and is estimated from simulation. The smaller reducible backgrounds with jets misidentified as leptons, e.g. $Z + \text{jets}$, are estimated from data.

In the $H \to ZZ \to 2\ell 2\nu$ search [87], we select events with a lepton pair (ee or $\mu\mu$), with invariant mass consistent with that of an on-shell Z boson, and large E_T^{miss}. We then define a transverse invariant mass m_T from the dilepton momenta and E_T^{miss}, assuming that E_T^{miss} arises from a $Z \to \nu\nu$ decay. We search for a broad excess of events in the m_T distribution. The non-resonant ZZ and WZ backgrounds are taken from simulation, while all other backgrounds are evaluated from control samples in data.

In the $H \to ZZ^{(*)} \to 2\ell 2q$ search [86], we select events with two leptons (ee or $\mu\mu$) and two jets with zero, one, or two b-tags, thus defining a total of six exclusive final states. Requiring b-tagging improves the signal-to-background ratio. The two jets are required to form an invariant mass consistent with that of an on-shell Z boson. The aim is to search for a peak in the invariant mass distribution of the dilepton-dijet system, with the background rate and shape estimated using control regions in data.

In the $H \to ZZ \to 2\ell 2\tau$ search [85], one Z boson is required to be on-shell and to decay to a lepton pair (ee or $\mu\mu$). The other Z boson is required to decay through a $\tau\tau$ pair to one of the four final-state signatures $e\mu$, $e\tau_h$, $\mu\tau_h$, $\tau_h\tau_h$. Thus, eight exclusive sub-channels are defined. We search for a broad excess in the distribution of the dilepton-ditau mass, constructed from the visible products of the tau decays, neglecting the effect of the accompanying neutrinos. The dominant background is non-resonant ZZ production whose rate is estimated from simulation. The main sub-leading backgrounds with jets misidentified as τ leptons stem from $Z + \text{jets}$ (including ZW) and top-quark events. These backgrounds are estimated from data.

Table 1: Summary information on the analyses included in this combination. All final states are exclusive. Notations used are: $(jj)_{VBF}$ stands for a dijet pair consistent with the VBF topology (VBF-tag); $(jj)_V$ – dijet pair with an invariant mass consistent with coming from a W or Z dijet decay; V – W and Z bosons; SF dileptons – ee or $\mu\mu$ pairs (same flavour); DF dileptons – $e\mu$ pairs (different flavour). The column "H prod" indicates which production mechanism is targeted by an analysis; it does not imply 100% purity (e.g. analyses targeting VBF are expected to have 30%-50% of their signal events coming from gluon-gluon fusion). The main contribution in the untagged and inclusive categories is always gluon-gluon fusion. When two references are given, they refer to the 7 TeV and 8 TeV analyses, respectively. When one reference is given for an analysis using both 7 TeV and 8 TeV data, the 7 TeV data have been re-analysed with improved analysis strategies and the new results may differ from the previously published results.

Analyses			No. of	m_H range	m_H	Lumi (fb^{-1})		Ref
H decay	H prod	Exclusive final states	channels	(GeV)	resolution	7 TeV	8 TeV	
$\gamma\gamma$	untagged	$\gamma\gamma$ (4 diphoton classes)	4	110–150	1-2%	5.1	5.3	[73]
	VBF-tag	$\gamma\gamma + (jj)_{VBF}$ (low or high m_{jj} for 8 TeV)	1 or 2	110–150	1-2%	5.1	5.3	[73]
bb	VH-tag	$(\nu\nu,\ ee,\ \mu\mu,\ e\nu,\ \mu\nu$ with 2 b-jets$)\otimes$ (low or high p_T^V)	10	110–135	10%	5.0	5.1	[74]
	$t\bar{t}$H-tag	(ℓ with 4,5,$\geq$6 jets) $\otimes$ (3,$\geq$4 b-tags); (ℓ with 6 jets with 2 b-tags); ($\ell\ell$ with 2 or $\geq$3 b-tagged jets)	9	110–140		5.0	-	[75]
$H \to \tau\tau$	0/1-jets	$(e\tau_h,\ \mu\tau_h,\ e\mu,\ \mu\mu)\times$ (low or high $p_T^{\tau\tau}$) $\times$ (0 or 1 jets)	16	110–145	20%	4.9	5.1	[76]
	VBF-tag	$(e\tau_h,\ \mu\tau_h,\ e\mu,\ \mu\mu) + (jj)_{VBF}$	4	110–145	20%	4.9	5.1	[76]
	ZH-tag	$(ee,\ \mu\mu) \times (\tau_h\tau_h,\ e\tau_h,\ \mu\tau_h,\ e\mu)$	8	110–160		5.0	-	[77]
	WH-tag	$\tau_h ee, \tau_h\mu\mu, \tau_h e\mu$	3	110–140		4.9	-	[78]
$WW \to \ell\nu qq$	untagged	$(e\nu,\ \mu\nu)\otimes((jj)_W$ with 0 or 1 jets)	4	170–600		5.0	5.1	[79, 80]
$WW \to \ell\nu\ell\nu$	0/1-jets	(DF or SF dileptons) $\otimes$ (0 or 1 jets)	4	110–600	20%	4.9	5.1	[81, 82]
$WW \to \ell\nu\ell\nu$	VBF-tag	$\ell\nu\ell\nu + (jj)_{VBF}$ (DF or SF dileptons for 8 TeV)	1 or 2	110–600	20%	4.9	5.1	[81, 82]
$WW \to \ell\nu\ell\nu$	WH-tag	$3\ell 3\nu$	1	110–200		4.9	-	[83]
$WW \to \ell\nu\ell\nu$	VH-tag	$\ell\nu\ell\nu + (jj)_V$ (DF or SF dileptons)	2	118–190		4.9	-	[84]
$ZZ \to 4\ell$	inclusive	$4e$, 4μ, $2e2\mu$	3	110–600	1-2%	5.0	5.3	[85]
$ZZ \to 2\ell 2\tau$	inclusive	$(ee,\ \mu\mu) \times (\tau_h\tau_h,\ e\tau_h,\ \mu\tau_h,\ e\mu)$	8	200–600	10-15%	5.0	5.3	[85]
$ZZ \to 2\ell 2q$	inclusive	$(ee, \mu\mu)\times((jj)_Z$ with 0, 1, 2 b-tags)	6	130–164 200–600	3%	4.9	-	[86]
$ZZ \to 2\ell 2\nu$	untagged	$((ee, \mu\mu)$ with MET) $\otimes$ (0 or 1 or 2 non-VBF jets)	6	200–600	7%	4.9	5.1	[87]
$ZZ \to 2\ell 2\nu$	VBF-tag	$(ee, \mu\mu)$ with MET and $(jj)_{VBF}$	2	200–600	7%	4.9	5.1	[87]

Table 2: Summary of production mechanisms and decay channels explicitly targeted in the searches for a low mass Higgs boson ($m_H < 135\,\text{GeV}$). Untagged searches include gluon-gluon fusion $gg \to H$ plus any phase space not covered by searches with explicit tags for enriching datasets with events from VBF, VH, and $t\bar{t}H$ production. V stands for W or Z. All analyses targeting a particular production mechanism are never 100% pure and have an admixture, sometimes very substantial, of other production mechanisms.

	untagged	VBF-tag	VH-tag	$t\bar{t}$H-tag
$H \to \gamma\gamma$	✓	✓		
$H \to b\bar{b}$			✓	✓
$H \to \tau\tau$	✓	✓	✓	
$H \to WW$	✓	✓	✓	
$H \to ZZ$	✓			

3 Combination methodology

The combination of the Higgs boson searches requires simultaneous analysis of the data selected by all individual analyses, accounting for all statistical and systematic uncertainties and their correlations. The overall statistical methodology used in this combination was developed by the ATLAS and CMS Collaborations in the context of the LHC Higgs Combination Group. The description of the general methodology can be found in Refs. [14, 89]. Below we give concise definitions of statistical quantities we use for characterizing the outcome of the search. Results presented in this note are obtained using asymptotic formulae [90], including a few updates recently introduced in the RooStats package [91].

3.1 Characterising the absence of a signal: limits

For calculations of exclusion limits, we adopt the modified frequentist criterion $\mathrm{CL_s}$ [92, 93]. The chosen test statistic q, used to determine how signal- or background-like the data are, is based on the profile likelihood ratio. Systematic uncertainties are incorporated in the analysis via nuisance parameters and are treated according to the frequentist paradigm. The profile likelihood ratio is defined as

$$q_\mu \;=\; -2\,\ln\frac{\mathcal{L}(\mathrm{obs}\,|\,\mu\cdot s+b,\,\hat{\hat{\theta}}_\mu)}{\mathcal{L}(\mathrm{obs}\,|\,\hat{\mu}\cdot s+b,\,\hat{\theta})}, \tag{1}$$

where s stands for the signal expected under the SM Higgs hypothesis, μ is a signal strength modifier introduced to accommodate deviations from SM Higgs predictions, b stands for backgrounds, and θ are nuisance parameters describing systematic uncertainties ($\hat{\hat{\theta}}_\mu$ maximizes the likelihood in the numerator for a given μ, while $\hat{\mu}$ and $\hat{\theta}$ define the point at which the likelihood reaches its global maximum).

The ratio of probabilities to observe a value of the test statistic at least as large as the one observed in data, q_μ^{obs}, under the signal+background (s+b) and background-only (b) hypotheses,

$$\mathrm{CL_s} = \frac{\mathrm{P}(q_\mu \geq q_\mu^{\mathrm{obs}}\,|\,\mu\cdot s+b)}{\mathrm{P}(q_\mu \geq q_\mu^{\mathrm{obs}}\,|\,b)} \;\leq \alpha, \tag{2}$$

is used as the criterion for excluding the signal at the $1-\alpha$ confidence level.

3.2 Characterising an excess of events: p-values and significance

To quantify the presence of an excess of events over what is expected for the background, we use the test statistic where the likelihood appearing in the numerator is for the background-only hypothesis:

$$q_0 \;=\; -2\,\ln\frac{\mathcal{L}(\mathrm{obs}\,|\,b,\,\hat{\hat{\theta}}_0)}{\mathcal{L}(\mathrm{obs}\,|\,\hat{\mu}\cdot s+b,\,\hat{\theta})}, \tag{3}$$

The statistical significance Z of a signal-like excess is computed from the probability p_0

$$p_0 = \mathrm{P}(q_0 \geq q_0^{obs}\,|\,\mathrm{b}), \tag{4}$$

henceforth referred to as the p-value, using the one-sided Gaussian tail convention.

$$p_0 = \int_Z^{+\infty} \frac{1}{\sqrt{2\pi}} \exp(-x^2/2)\ \mathrm{d}x. \tag{5}$$

In the Higgs boson search, we scan over Higgs boson mass hypotheses and look for the one giving the minimum local p-value $p^{\min}_{\text{local}}$, which describes the probability of a background fluctuation for that particular Higgs boson mass hypothesis. The probability to find a fluctuation with a local p-value lower or equal to the observed $p^{\min}_{\text{local}}$ anywhere in the explored mass range is referred to as the global p-value, p_{global}:

$$p_{\text{global}} = \mathrm{P}(p_0 \leq p^{\min}_{\text{local}} \,|\, \mathrm{b}), \tag{6}$$

The fact that the global p-value can be significantly larger than $p^{\min}_{\text{local}}$ is often referred to as the look-elsewhere effect (LEE). The global significance (and global p-value) of the observed excess can be evaluated in this case by generating pseudo-datasets, which, however, becomes too CPU-intensive and not practical for very small p-values. Therefore, we use the method suggested in Ref. [94]. The relationship between global and local p-values is given by:

$$p_{\text{global}} = p^{\min}_{\text{local}} + C \cdot e^{-Z^2_{\text{local}}/2} \tag{7}$$

The constant C is found by generating a relatively small set of pseudo-data and then is used to evaluate the global p-value corresponding to $p^{\min}_{\text{local}}$ observed in the experiment.

For a very wide mass range, the constant C can be evaluated directly from data [89] by counting upcrossings N_{up} of $\hat{\mu}(m_{\text{H}})$ with the line $\mu = 0$ and setting $C = N_{\text{up}}$.

3.3 Extracting signal model parameters

Signal model parameters a (signal strength modifier μ can be one of them) are evaluated from a scan of the profile likelihood ratio $q(a)$:

$$q(a) = -2 \ln \frac{\mathcal{L}(\text{obs} \,|\, s(a) + b,\, \hat{\theta}_a)}{\mathcal{L}(\text{obs} \,|\, s(\hat{a}) + b,\, \hat{\theta})}, \tag{8}$$

Parameters $\hat{a}$ and $\hat{\theta}$ that maximize the likelihood, $\mathcal{L}(\text{obs} \,|\, s(\hat{a}) + b,\, \hat{\theta}) = \mathcal{L}_{\max}$, are called the best-fit set. The 68% (95%) CL on a given parameter of interest a_i is evaluated from $q(a_i) = 1$ (3.84) with all other unconstrained model parameters treated in the same way as the nuisance parameters. The 2D 68% (95%) CL contours for pairs of parameters are derived from $q(a_i, a_j) = 2.3$ (6). One should keep in mind that boundaries of 2D confidence regions projected on either parameter axis are not identical to the 1D confidence interval for that parameter.

4 Search results

4.1 Exclusion limits on the SM Higgs boson

The CL_s value for the SM Higgs boson hypothesis as a function of its mass is shown in Fig. 3. The observed values are shown by the solid line. The dashed black line indicates the median of the expected results for the background-only hypothesis, with the green (dark) and yellow (light) bands indicating the ranges in which the CL_s values are expected to reside in 68% and 95% of the experiments under the background-only hypothesis. The probabilities for an observation to lie above or below the 68% (95%) band are 16% (2.5%) each. The thick red horizontal lines indicate CL_s values of 0.10, 0.05, and 0.01. The mass regions where the observed CL_s values are below these lines are excluded with the corresponding $(1 - CL_s)$ confidence levels of 90%, 95%, and 99%, respectively. We exclude a SM Higgs boson at 95% CL in two mass ranges 110 – 122.5 GeV and 127– 600 GeV. At 99% CL, we exclude it in three mass ranges 110–112 GeV, 113–121.5 GeV, and 128–600 GeV.

Figure 4 shows the 95% CL upper limits on the signal strength modifier, $\mu = \sigma/\sigma_{\mathrm{SM\,H}}$ as a function of m_{H}. The ordinate thus shows the Higgs boson cross section that is excluded at 95% CL, expressed as a multiple of the SM Higgs boson cross section.

The median expected exclusion range of m_{H} at 95% CL in the absence of a signal is 110–600 GeV. In most of the explored Higgs boson mass range, the differences between the observed and expected limits are consistent with statistical fluctuations since the observed limits are generally within the green (68%) or yellow (95%) bands of the expected limit values. However at low mass, in the range $122.5 < m_{\mathrm{H}} < 127$ GeV, we observe an excess of events which makes the observed limits considerably weaker than expected in the absence of a SM Higgs boson and, hence, does not allow exclusion.

4.2 Significance of the observed excess

To quantify the consistency of the observed excesses with the background-only hypothesis, we show in Fig. 5 (left) a scan of the local p-value p_0 in the low-mass region for 7 TeV, 8 TeV, and the overall combination. Both 7 TeV and 8 TeV datasets exhibit excesses, 3.0σ and 3.8σ, respectively, for a Higgs boson mass around 125 GeV. In the overall combination, this results in a 4.9σ excess, with a corresponding local p-value of $p_{\mathrm{min}} = 5.5 \times 10^{-7}$.

Fig. 5 (right) gives p-values for sub-combinations by decay channel. The largest contributors to the overall excess in the combination are the $\gamma\gamma$ and $ZZ \to 4\ell$ channels. They both have very good mass resolution and allow for a good localization of the invariant mass of a putative resonance that might be responsible for the excess. Their combined significance reaches 5.0σ (Fig. 6 (left)).

The WW channel has a comparable exclusion sensitivity to the $\gamma\gamma$ and $ZZ \to 4\ell$ channels, but does not have a good mass resolution. Fig. 5 (right) shows that it has a modest excess with a local significance of 1.5σ for $m_{\mathrm{H}} \sim 125$ GeV. When added to the $\gamma\gamma$ and $ZZ \to 4\ell$ channels, the combined significance becomes 5.1σ (Fig. 6 (right)).

The bb and $\tau\tau$ channels do not show any excess for $m_{\mathrm{H}} \sim 125$ GeV. After including them in the combination, the final significance becomes 4.9σ, as stated above.

Figure 7 shows the two separate combinations for the 7 and 8 TeV datasets in the low-mass range. The overall channel-by-channel pattern of observed excesses in both datasets is consistent.

The LEE-corrected significance in a search range of 115–130 (110–145) GeV is evaluated by generating about 10 000 pseudo-observations. After fitting for constant C in the relationship between global and minimum local p-values (Eq. (7)), we find that the global p-values in these ranges remain very high: 4.5σ (4.4σ). The global significance of the excess in the full search mass range 110–600 GeV is estimated by counting the number of transitions from deficit to excess over this range; it is also found to remain very high: 4.0σ.

These tests confirm that the observed excess with a local significance of 4.9σ cannot be explained by a statistical fluctuation in the data. Together with the compatibility of the observations in the 7 TeV and 8 TeV datasets, this leads us to believe that we observe a new state with a mass near 125 GeV, manifesting itself in our analyses via its decays to two photons and four leptons. For these two decay modes, individually, we observe a signal with significances of 4.1σ in the $\gamma\gamma$ decay mode and 3.2σ in the 4ℓ decay mode.

4.3 Mass of the observed state

To measure the mass of the observed state, we use the $\gamma\gamma$ and $ZZ \to 4\ell$ channels that have excellent mass resolution (Table 1) and for which we observe the excess with a high significance. Figure 8 (left) shows 2D 68% confidence level regions for two parameters of interest, the signal strength μ and mass m_X for the three channels (untagged $\gamma\gamma$, VBF-tagged $\gamma\gamma$, and $ZZ \to 4\ell$). The three channels are consistent and thus can be combined. The combined 68% CL contour shown with a black line in Fig. 8 (left) assumes that the relative event yields between the three channels are fixed to the standard model expectation, while the overall signal strength is a free parameter.

To extract the value of m_X in a model-independent way, the untagged $\gamma\gamma$, VBF-tagged $\gamma\gamma$, and $ZZ \to 4\ell$ channels are treated independently, each with their own signal cross sections. Technically, this is achieved by scaling the expected event yields in these channels by independent factors μ_i, where i stands for untagged $\gamma\gamma$, VBF-tagged $\gamma\gamma$, and $ZZ \to 4\ell$. The signal is assumed to be due to a state with a unique mass m_X. The mass m_X and its uncertainty are extracted from a scan of the combined test statistic $q(m_X)$ with signal strengths μ_i profiled in the same way as for all other nuisance parameters. Figure 8 shows the test statistic scan as a function of the hypothesised mass m_X for the three final states separately and their combination. Scans of the test statistic with profiled and fixed nuisance parameters allow us to extract both the total and statistical uncertainties on the mass. The quadrature difference gives the overall systematic error. The combined best-fit mass is $m_X = 125.3 \pm 0.4\,(\text{stat}) \pm 0.5\,(\text{syst})$ GeV.

4.4 Compatibility of the observed state with the SM Higgs boson hypothesis

The p-value characterises the probability of background producing an observed excess of events, but it does not give information about the compatibility of an excess with an expected signal. The current amount of data allows only for a limited number of such compatibility tests, which we present in this subsection. These compatibility tests do not constitute measurements of any physics parameters per se, but rather show the consistency of the various observations with the expectations for the SM Higgs boson.

The best fit value for the common signal strength modifier $\hat{\mu} = \sigma/\sigma_{\text{SM H}}$, obtained in a combination of all search channels, provides the first compatibility test. Figure 9 shows a scan of the overall $\hat{\mu}$ obtained in the combination of all channels versus the hypothesised Higgs boson mass m_H. The band corresponds to the $\pm 1\sigma$ uncertainty (statistical+systematic). The excesses seen in the 7 TeV and 8 TeV data, and in their combination, around 125 GeV are consistent with $\mu = 1$ within the $\pm 1\sigma$ uncertainties. The observed $\hat{\mu}$ value for an excess around 125 GeV in the

combination of all data is found to be 0.80 ± 0.22.

Figures 10 and 11 show the consistency of the $\hat{\mu}$ values obtained for the different sub-combinations. Figure 10 shows the interplay of the 11 sub-combinations given in Table 2. Figure 11 presents sub-combinations by decay mode and production mechanism. The plots show a satisfactory level of compatibility between all the channels contributing to the combination and between results obtained for the 7 and 8 TeV datasets. None of the sub-combinations depart from the best-fit value of the overall signal strength modifier by a significant deviation with respect to their current individual sensitivities.

Electroweak symmetry breaking via the Higgs mechanism sets a well-defined ratio for the couplings of the Higgs boson to the W and Z bosons, $g_{\mathrm{HWW}}/g_{\mathrm{HZZ}}$, protected by the custodial symmetry. The dominant production mechanism populating the inclusive $pp \to \mathrm{H} \to \mathrm{ZZ}$ and untagged $pp \to \mathrm{H} \to \mathrm{WW}$ search channels is $gg \to \mathrm{H}$. Therefore the ratio of event yields in these channels provides a natural test of the custodial symmetry. To quantify such consistency, we introduce two event rate modifiers μ_{ZZ} and R_{wz}. The expected $H \to \mathrm{ZZ} \to 4\ell$ event yield is scaled by μ_{ZZ}, while the expected untagged $H \to \mathrm{WW} \to \ell\nu\ell\nu$ event yield is scaled by $R_{wz} \cdot \mu_{ZZ}$. The mass of the observed state is fixed to the best-fit mass value of 125.3 GeV. A scan of the test statistic $q(R_{wz})$, while profiling all other nuisances and the signal strength modifier μ_{ZZ}, yields $R_{wz} = 0.9\ ^{+1.1}_{-0.6}$. The contribution from VBF and VH signal production to the inclusive selection gives a small bias when relating the observed event yield ratio R_{wz} to the ratio of the couplings. We find that the bias is about 0.02, which is much smaller than the current statistical precision of the measurement. Hence, the current observations, albeit with limited statistical precision, are consistent with the expectation set by the custodial symmetry.

Given that R_{wz} is consistent with unity, we now assume that the ratio of the couplings of the observed state to the W and Z bosons is as required by the custodial symmetry. Under this assumption, we can check the compatibility of the observation with the standard model Higgs boson by introducing and fitting for two free parameters c_V and c_F. The first, c_V, scales the standard model Higgs boson couplings to the W and Z bosons, while preserving their ratio. The other, c_F, scales all couplings to fermions by one constant factor. At LO, all partial widths, except for $\Gamma_{\gamma\gamma}$, scale either as c_V^2 or c_F^2. The partial width $\Gamma_{\gamma\gamma}$ is induced via loop diagrams, with the W boson and top quark being the dominant contributors; hence, it scales as $|\alpha\, c_V + \beta\, c_F|^2$, where factors $\alpha(m_{\mathrm{H}})$ and $\beta(m_{\mathrm{H}})$ are taken from predictions for the SM Higgs boson [31]. Then, the event yield in any production$\times$decay mode can be easily rescaled for any $c_V \neq 1$ and/or $c_F \neq 1$, starting from the following equation:

$$N(xx \to \mathrm{H} \to yy) \sim \frac{\Gamma_{xx}\,\Gamma_{yy}}{\Gamma_{\mathrm{tot}}}. \tag{9}$$

In this equation Γ_{tot} is also a function of c_V and c_F; it is calculated as the sum of the rescaled partial widths. As before, the c_V and c_F re-scaling factors do not represent any particular physics model and serve the sole purpose of testing the compatibility of the observation with the standard model Higgs boson hypothesis. The 2D likelihood scan and the 68% and 95% confidence regions for c_V and c_F are shown in Fig. 12. In this scan, c_V and c_F are constrained to be positive. We note that formally there is another deeper minimum in the likelihood in the $(+,-)$ quadrant, but we do not consider this quadrant as it has no physics meaning in the context of the (c_V,c_F)-parametrisation. One can see that the data are compatible with the expectation for the standard model Higgs boson: the point (c_V, c_F)=(1,1) is within the 95% confidence interval defined by data. The best-fit values are (c_V, c_F)=(1.0 ,0.5). The 1D 95% CL intervals for c_V and c_F, if the other parameter is fixed to unity, are [0.7; 1.2] and [0.3; 1.0], respectively.

5 Conclusions

Combined results are presented from searches for the standard model (SM) Higgs boson in proton-proton collisions at $\sqrt{s} = 7$ and 8 TeV in five decay modes: $\gamma\gamma$, bb, $\tau\tau$, WW, and ZZ. The analysed data correspond to integrated luminosities of up to 5.1 fb^{-1} at 7 TeV and 5.3 fb^{-1} at 8 TeV. The data exclude the existence of a SM Higgs boson in the ranges 110–122.5 and 127–600 GeV at 95% confidence level. An excess of events above the expected SM background is observed with a local significance of 4.9σ around 125 GeV, which we attribute to the production of a previously unobserved particle. The evidence is strongest in the two final states with the best mass resolution: the two-photon final state and the final state with two pairs of charged leptons (electrons or muons). The combined excess in these channels alone gives a local significance of 5.0σ. An unconstrained fit to the excesses in these two final states yields a mass of $125.3 \pm 0.4\,(\text{stat}) \pm 0.5\,(\text{syst})$ GeV. Within the statistical uncertainties, the results obtained in all search channels are consistent with the expectations for a SM Higgs boson. More data are needed to test whether the properties of this new state are indeed those of the SM Higgs boson or whether some differ, implying new physics beyond the standard model.

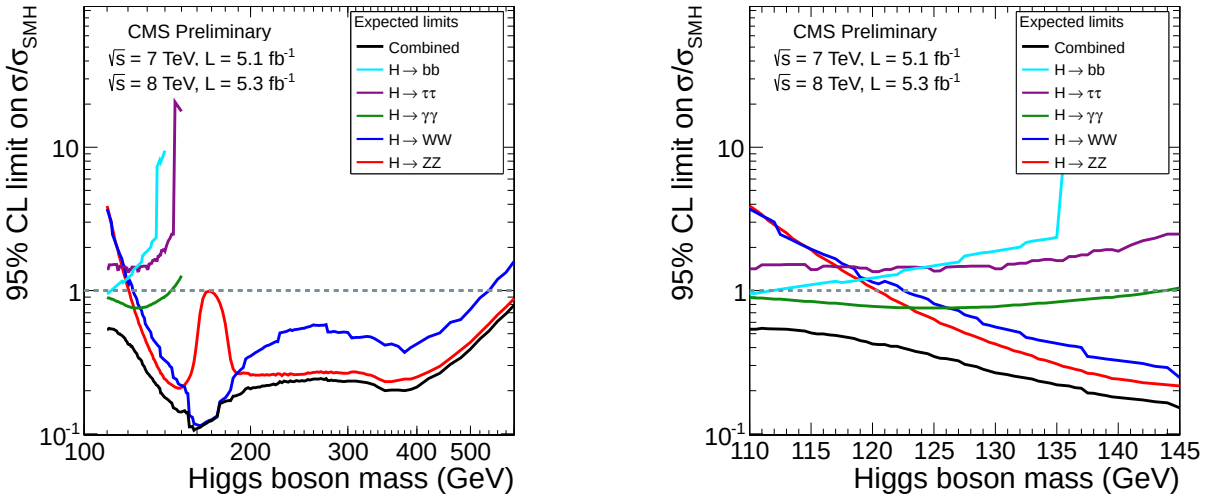

Figure 1: The median expected 95% CL upper limits on the cross section ratio $\sigma/\sigma_{\mathrm{SM\,H}}$ in the absence of a Higgs boson as a function of the SM Higgs boson mass in the range 110–600 GeV (left) and 110–145 GeV (right), for the five Higgs boson decay channels. Here $\sigma_{\mathrm{SM\,H}}$ denotes the cross section predicted for the SM Higgs boson. A channel showing values below unity (dashed horizontal line) would be expected to be able to exclude a Higgs boson of that mass at 95% CL. The jagged structure in the limits for some channels results from the different event selection criteria employed in those channels for different Higgs boson mass sub-ranges.

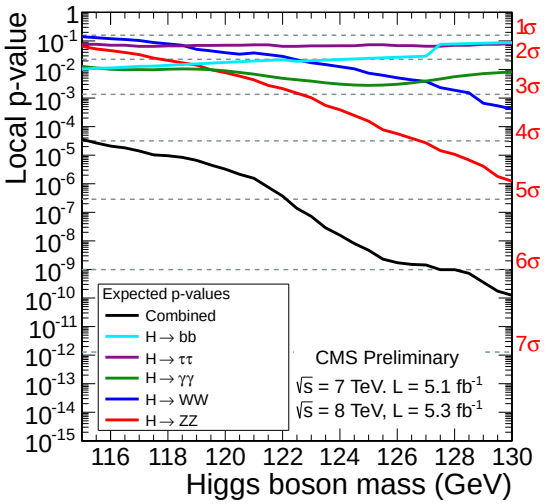

Figure 2: The median expected p-value for observing an excess at mass m_{H} assuming that the SM Higgs boson with that mass exists, as a function of the SM Higgs boson mass in the range 110–130 GeV. Expectations for sub-combinations in five Higgs boson decay channels and the overall combination are shown.

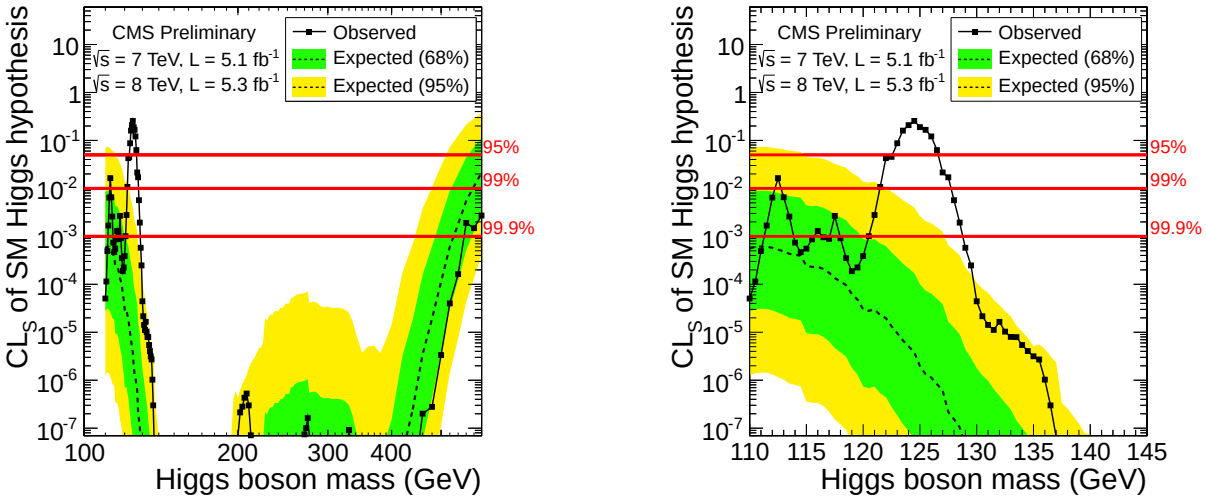

Figure 3: The CL_s values for the SM Higgs boson hypothesis as a function of the Higgs boson mass in the range 110–600 GeV (left) and 110–145 GeV (right).

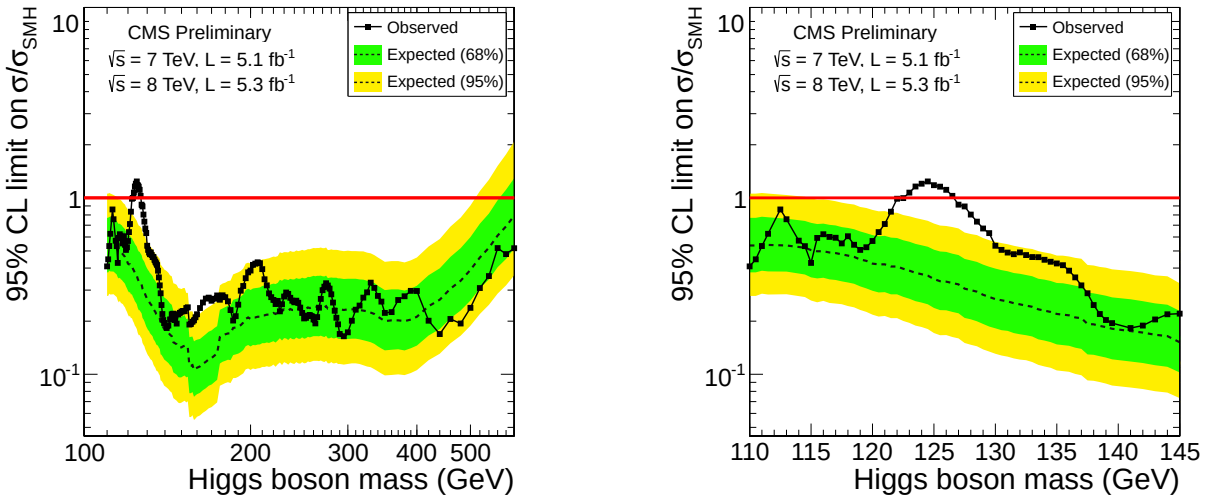

Figure 4: The 95% CL upper limits on the signal strength parameter $\mu = \sigma/\sigma_{\mathrm{SM\,H}}$ for the SM Higgs boson hypothesis as a function of the Higgs boson mass in the range 110–600 GeV (left) and 110–145 GeV (right).

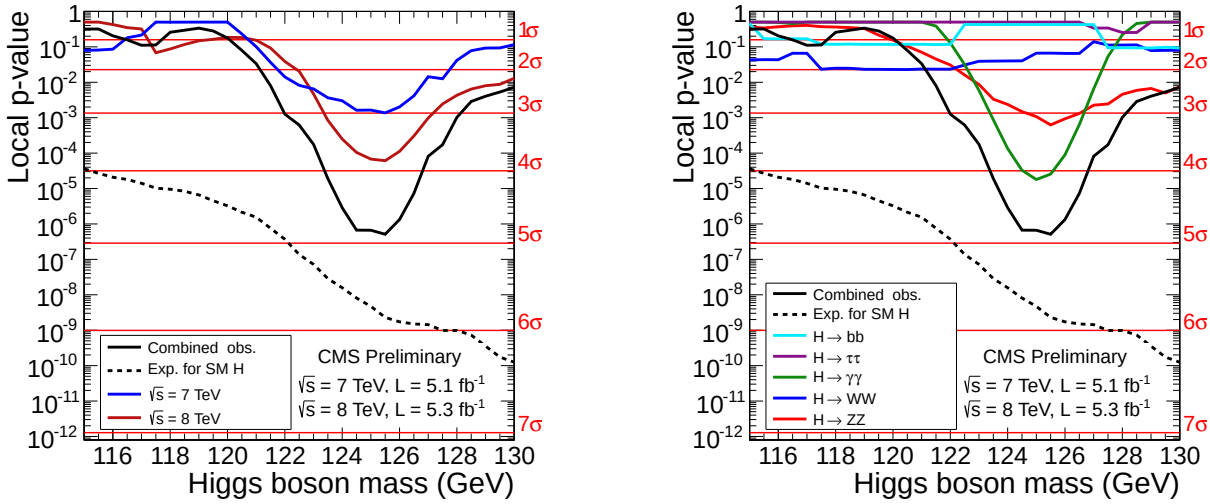

Figure 5: (left) The observed local p-value p_0 for 7-TeV, 8-TeV data, and their combination as a function of the Higgs boson mass. (right) The observed local p-value p_0 for five sub-combinations by decay mode and the overall combination as a function of the Higgs boson mass. The dashed lines show the expected local p-values $p_0(m_{\mathrm{H}})$, should a SM Higgs boson with a mass m_{H} exist.

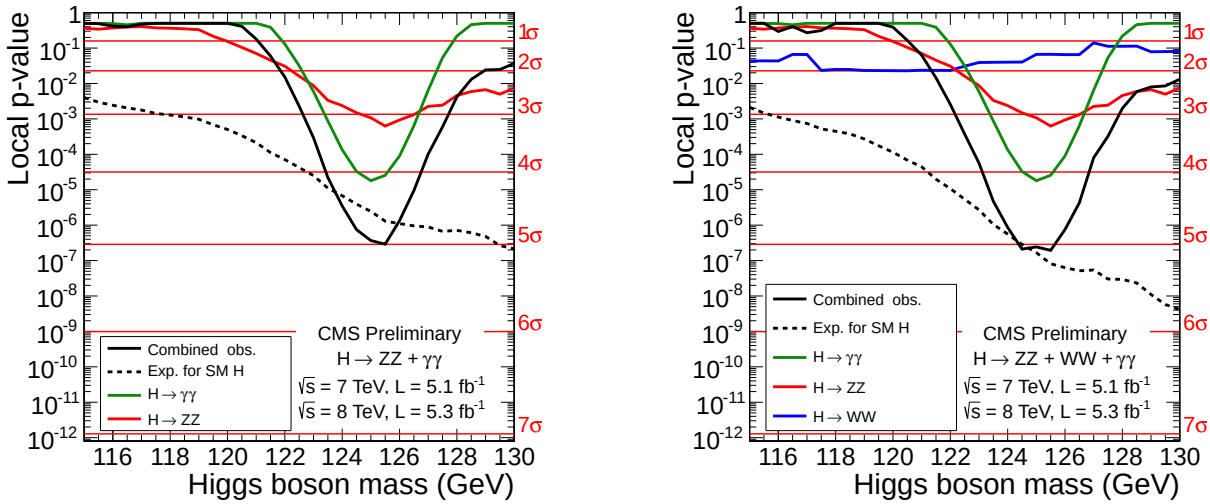

Figure 6: (left) The observed local p-value for decay modes with good mass resolution channels, $\gamma\gamma$ and ZZ $\to 4\ell$, as a function of the Higgs boson mass. (right) The observed local p-value for the bosonic decay modes, $\gamma\gamma$, ZZ $\to 4\ell$, and WW $\to \ell\nu\ell\nu$, as a function of the Higgs boson mass. The dashed lines show the expected local p-values $p_0(m_{\mathrm{H}})$, should a SM Higgs boson with a mass m_{H} exist.

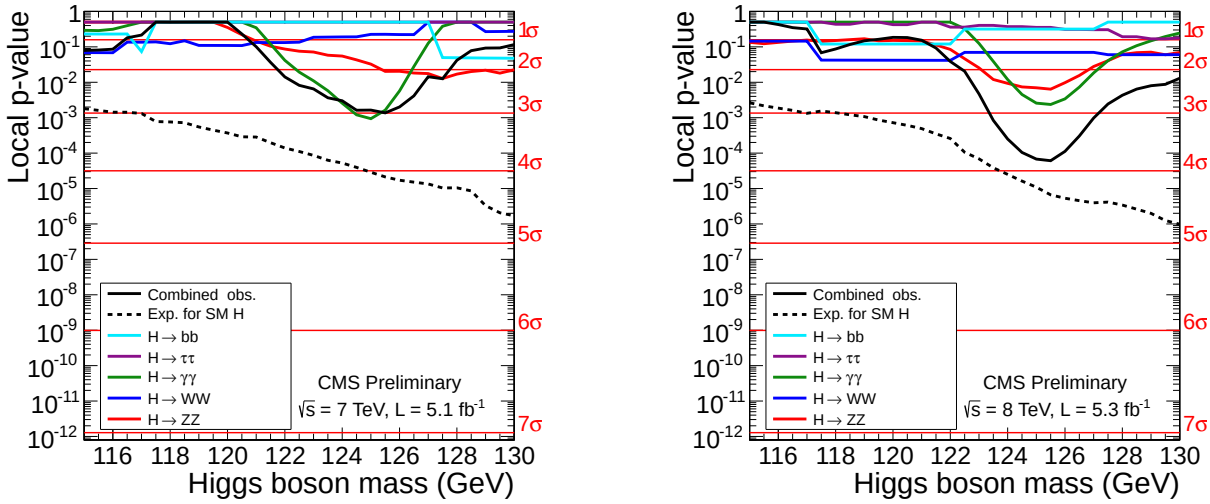

Figure 7: The observed local p-value p_0 as a function of m_{H}, separately for searches with the 7 TeV (left) and 8 TeV (right) datasets. The dashed lines show the expected local p-values $p_0(m_{\mathrm{H}})$, should a SM Higgs boson with a mass m_{H} exist.

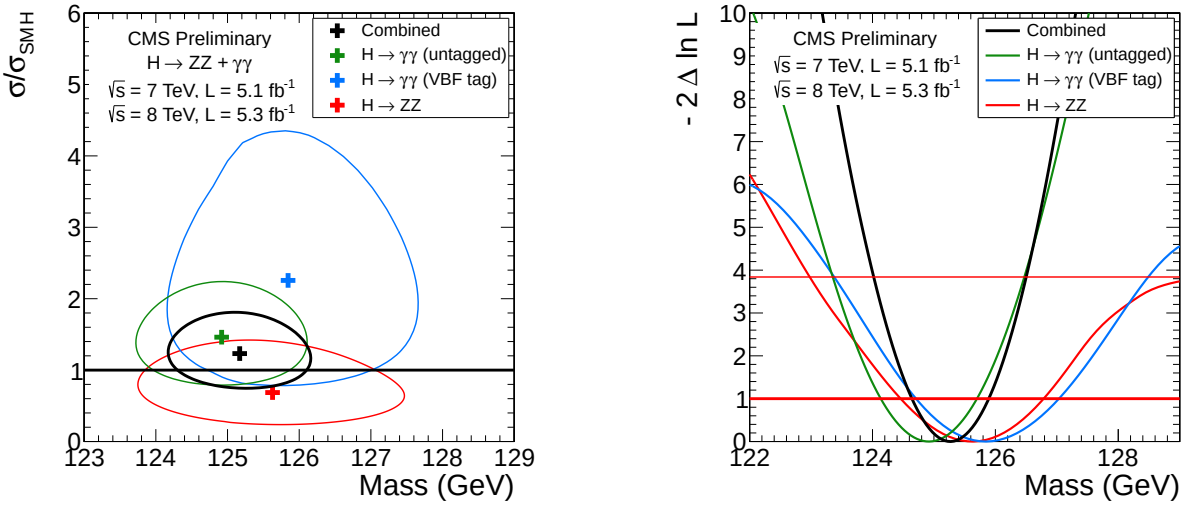

Figure 8: (Left) 2D 68% CL contours for a hypothesised Higgs boson mass m_{H} and $\mu = \sigma/\sigma_{\mathrm{SM\,H}}$ for the untagged $\gamma\gamma$, VBF-tagged $\gamma\gamma$, and 4ℓ, and their combination. In this combination, the relative signal strengths for the three final states are fixed to the SM expectation. (Right) 1D test statistic $q(m_{\mathrm{X}})$ scan vs hypothesised Higgs boson mass m_{H} for the untagged $\gamma\gamma$, VBF-tagged $\gamma\gamma$, and 4ℓ final states separately and for their combination. In this combination, the signal strengths for the untagged $\gamma\gamma$, VBF-tagged $\gamma\gamma$, and 4ℓ final states are not constrained to the SM expectation.

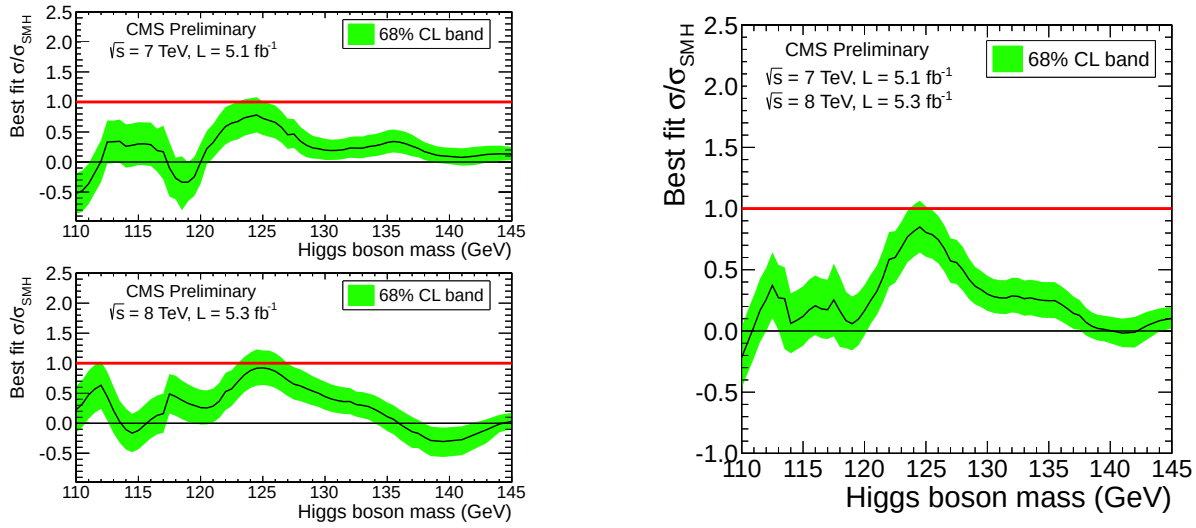

Figure 9: The observed best-fit $\hat{\mu} = \sigma/\sigma_{\mathrm{SM\,H}}$ as a function of the SM Higgs boson mass in the range 110–145 GeV for the 7 and 8 TeV datasets separately (left) and combined (right). The bands correspond to the $\pm 1\sigma$ uncertainties (statistical and systematic combined) on the $\hat{\mu}$ values.

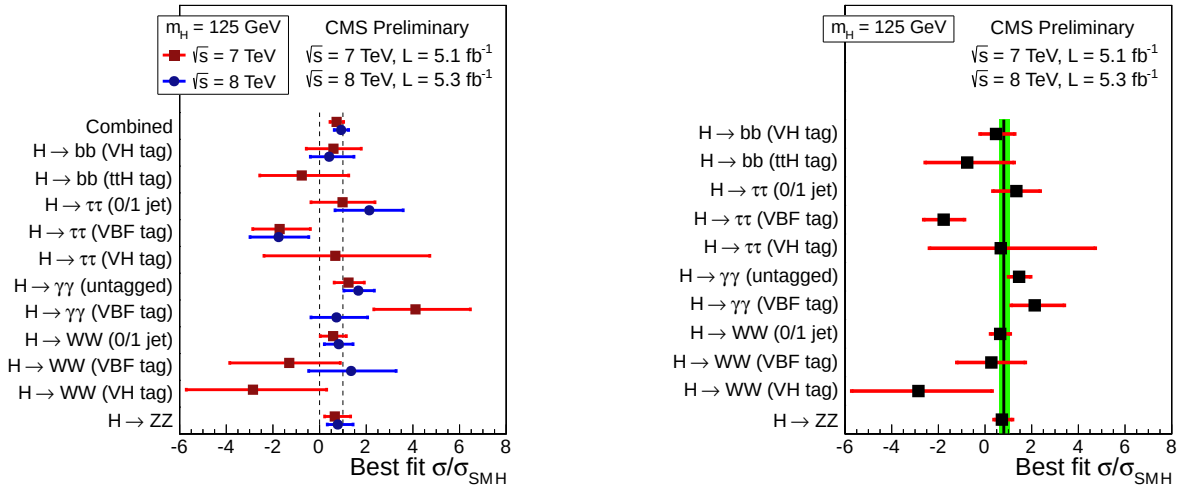

Figure 10: Values of $\hat{\mu} = \sigma/\sigma_{\mathrm{SM\,H}}$ for the combination (solid vertical line) and for contributing channels (points) for the 7 and 8 TeV datasets separately (left) and for their combination (right). The vertical band shows the overall $\hat{\mu}$ value 0.80 ± 0.22. The horizontal bars indicate the $\pm 1\sigma$ uncertainties on the $\hat{\mu}$ values for individual channels; they include both statistical and systematic uncertainties.

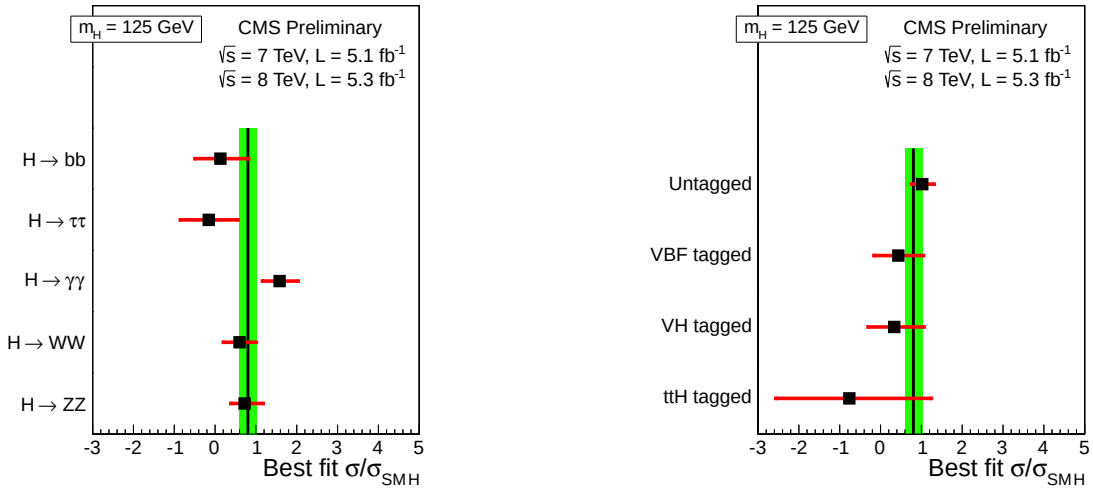

Figure 11: Values of $\hat{\mu} = \sigma/\sigma_{\mathrm{SM\,H}}$ for the combination (solid vertical line) and for sub-combinations (points) grouped by decay mode (left) and by a signature enhancing a specific production mechanism (right). The vertical band shows the overall $\hat{\mu}$ value 0.80 ± 0.22. The horizontal bars indicate the $\pm 1\sigma$ uncertainties on the $\hat{\mu}$ values for individual channels; they include both statistical and systematic uncertainties.

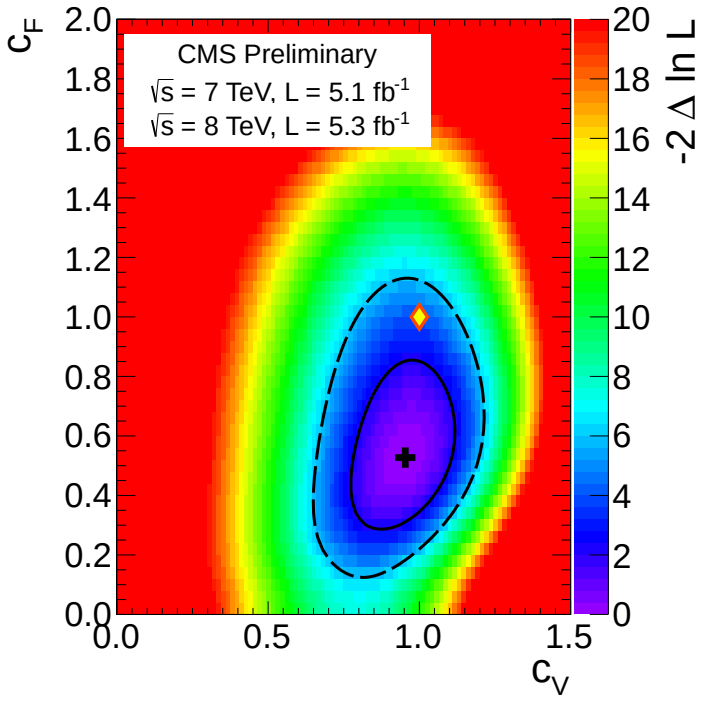

Figure 12: The 2D-scan of the test statistic $(-2 \ln Q)$ vs the (c_V, c_F) parameters. The cross indicates the best-fit values. The solid and dashed contours show the 68% and 95% CL ranges, respectively. The yellow diamond shows the SM point $(c_V, c_F) = (1, 1)$.

References

[1] S. Glashow, "Partial Symmetries of Weak Interactions", *Nucl. Phys.* **22** (1961) 579–588, doi:10.1016/0029-5582(61)90469-2.

[2] S. Weinberg, "A Model of Leptons", *Phys. Rev. Lett.* **19** (1967) 1264–1266, doi:10.1103/PhysRevLett.19.1264.

[3] A. Salam, "Weak and electromagnetic interactions", in *Elementary particle physics: relativistic groups and analyticity*, N. Svartholm, ed., p. 367. Almquvist & Wiskell, 1968. Proceedings of the eighth Nobel symposium.

[4] F. Englert and R. Brout, "Broken symmetry and the mass of gauge vector mesons", *Phys. Rev. Lett.* **13** (1964) 321–323, doi:10.1103/PhysRevLett.13.321.

[5] P. W. Higgs, "Broken symmetries, massless particles and gauge fields", *Phys. Lett.* **12** (1964) 132–133, doi:10.1016/0031-9163(64)91136-9.

[6] P. W. Higgs, "Broken symmetries and the masses of gauge bosons", *Phys. Rev. Lett.* **13** (1964) 508–509, doi:10.1103/PhysRevLett.13.508.

[7] G. Guralnik, C. Hagen, and T. W. B. Kibble, "Global conservation laws and massless particles", *Phys. Rev. Lett.* **13** (1964) 585–587, doi:10.1103/PhysRevLett.13.585.

[8] P. W. Higgs, "Spontaneous symmetry breakdown without massless bosons", *Phys. Rev.* **145** (1966) 1156–1163, doi:10.1103/PhysRev.145.1156.

[9] T. W. B. Kibble, "Symmetry breaking in non-Abelian gauge theories", *Phys. Rev.* **155** (1967) 1554–1561, doi:10.1103/PhysRev.155.1554.

[10] ALEPH, CDF, D0, DELPHI, L3, OPAL, SLD Collaborations, the LEP Electroweak Working Group, the Tevatron Electroweak Working Group, and the SLD Electroweak and Heavy Flavour Groups, "Precision Electroweak Measurements and Constraints on the Standard Model", CERN PH-EP-2010-095, (2010). At this time, the most up to date Higgs boson mass constraints come from http://lepewwg.web.cern.ch/LEPEWWG/plots/winter2012/.

[11] ALEPH, DELPHI, L3, OPAL Collaborations, and LEP Working Group for Higgs Boson Searches, "Search for the standard model Higgs boson at LEP", *Phys. Lett. B* **565** (2003) 61–75, doi:10.1016/S0370-2693(03)00614-2.

[12] CDF and D0 Collaborations, "Combination of Tevatron Searches for the Standard Model Higgs Boson in the WW Decay Mode", *Phys. Rev. Lett.* **104** (2010) 061802, doi:10.1103/PhysRevLett.104.061802.

[13] CDF and D0 Collaborations, "Updated Combination of CDF and D0 Searches for Standard Model Higgs Boson Production with up to 10.0 fb^{-1} of Data", (July, 2012). arXiv:1207.0449. FERMILAB-CONF-12-318-E; CDF Note 10884; D0 Note 6348.

[14] CMS Collaboration, "Combined results of searches for the standard model Higgs boson in pp collisions at $\sqrt{s}$ = 7 TeV", *Phys.Lett.* **B710** (2012) 26–48, arXiv:1202.1488.

[15] ATLAS Collaboration, "Combined search for the Standard Model Higgs boson using up to 4.9 fb^{-1} of pp collision data at $\sqrt{s}$ = 7 TeV with the ATLAS detector at the LHC", *Phys.Lett.* **B710** (2012) 49–66, arXiv:1202.1408.

[16] CMS Collaboration, "Combined results of searches for a Higgs boson in the context of the standard model and beyond-standard models", *CMS Physics Analysis Summary* **CMS-PAS-HIG-12-008** (2012).

[17] ATLAS Collaboration, "Combined search for the Standard Model Higgs boson in pp collisions at sqrt(s) = 7 TeV with the ATLAS detector", *CERN-PH-EP-2012-167, Submitted to Phys. Rev. D* (July, 2012).

[18] CMS Collaboration, "The CMS experiment at the CERN LHC", *JINST* **03** (2008) S08004, doi:10.1088/1748-0221/3/08/S08004.

[19] Ellis, John R. et al., "A Phenomenological Profile of the Higgs Boson", *Nucl.Phys. B* **106** (1976) 292.

[20] Georgi, H.M. et al., "Higgs Bosons from Two Gluon Annihilation in Proton Proton Collisions", *Phys.Rev.Lett.* **40** (1978) 692, doi:10.1103/PhysRevLett.40.692.

[21] Glashow, S.L. et al., "Associated Production of Higgs Bosons and Z Particles", *Phys.Rev.* **D18** (1978) 1724–1727, doi:10.1103/PhysRevD.18.1724.

[22] R. N. Cahn, S. D. Ellis, R. Kleiss et al., "Transverse Momentum Signatures for Heavy Higgs Bosons", *Phys.Rev.* **D35** (1987) 1626, doi:10.1103/PhysRevD.35.1626.

[23] D. L. Rainwater and D. Zeppenfeld, "Searching for H $\to$ gamma gamma in weak boson fusion at the LHC", *JHEP* **9712** (1997) 005, doi:10.1088/1126-6708/1997/12/005, arXiv:hep-ph/9712271.

[24] D. L. Rainwater, D. Zeppenfeld, and K. Hagiwara, "Searching for H $\to \tau\tau$ in weak boson fusion at the CERN LHC", *Phys. Rev. D* **59** (1998) 014037, doi:10.1103/PhysRevD.59.014037, arXiv:hep-ph/9808468.

[25] D. L. Rainwater and D. Zeppenfeld, "Observing H $\to W^{(*)}W^{(*)} \to e^{\pm}\mu^{\pm}$+missing-p(T) in weak boson fusion with dual forward jet tagging at the CERN LHC", *Phys. Rev. D* **60** (1999) 113004, doi:10.1103/PhysRevD.61.099901,10.1103/PhysRevD.60.113004, arXiv:hep-ph/9906218.

[26] LHC Higgs Cross Section Working Group, S. Dittmaier, C. Mariotti et al., "Handbook of LHC Higgs Cross Sections: 1. Inclusive Observables", *CERN-2011-002* (CERN, Geneva, 2011) arXiv:1101.0593.

[27] LHC Higgs Cross Section Working Group, S. Dittmaier, C. Mariotti et al., "Handbook of LHC Higgs Cross Sections: 2. Differential Distributions", *CERN-2012-002* (CERN, Geneva, 2012) arXiv:1201.3084.

[28] LHC Higgs Cross Section Working Group, "Higgs Cross Sections at 7 and 8 TeV", *https://twiki.cern.ch/twiki/bin/view/LHCPhysics/CrossSections*.

[29] Djouadi, A., Spira, M. and Zerwas, P. M., "Production of Higgs bosons in proton colliders: QCD corrections", *Phys. Lett. B* **264** (1991) 440–446, doi:10.1016/0370-2693(91)90375-Z.

[30] S. Dawson, "Radiative corrections to Higgs boson production", *Nucl. Phys. B* **359** (1991) 283–300, doi:10.1016/0550-3213(91)90061-2.

[31] Spira, M. et al., "Higgs boson production at the LHC", *Nucl. Phys. B* **453** (1995) 17–82, doi:10.1016/0550-3213(95)00379-7, arXiv:hep-ph/9504378.

[32] R. V. Harlander and W. B. Kilgore, "Next-to-next-to-leading order Higgs production at hadron colliders", *Phys. Rev. Lett.* **88** (2002) 201801, doi:10.1103/PhysRevLett.88.201801, arXiv:hep-ph/0201206.

[33] C. Anastasiou and K. Melnikov, "Higgs boson production at hadron colliders in NNLO QCD", *Nucl. Phys. B* **646** (2002) 220–256, doi:10.1016/S0550-3213(02)00837-4, arXiv:hep-ph/0207004.

[34] V. Ravindran, J. Smith, and W. L. van Neerven, "NNLO corrections to the total cross section for Higgs boson production in hadron hadron collisions", *Nucl. Phys. B* **665** (2003) 325–366, doi:10.1016/S0550-3213(03)00457-7, arXiv:hep-ph/0302135.

[35] S. Catani et al., "Soft-gluon resummation for Higgs boson production at hadron colliders", *JHEP* **07** (2003) 028, doi:10.1088/1126-6708/2003/07/028.

[36] U. Aglietti et al., "Two-loop light fermion contribution to Higgs production and decays", *Phys. Lett. B* **595** (2004) 432–441, doi:10.1016/j.physletb.2004.06.063, arXiv:hep-ph/0404071.

[37] Degrassi, G. and Maltoni, F., "Two-loop electroweak corrections to Higgs production at hadron colliders", *Phys. Lett. B* **600** (2004) 255–260, doi:10.1016/j.physletb.2004.09.008, arXiv:hep-ph/0407249.

[38] S. Actis et al., "NLO Electroweak Corrections to Higgs Boson Production at Hadron Colliders", *Phys. Lett. B* **670** (2008) 12–17, doi:10.1016/j.physletb.2008.10.018, arXiv:0809.1301.

[39] C. Anastasiou et al., "Mixed QCD-electroweak corrections to Higgs boson production in gluon fusion", *JHEP* **04** (2009) 003, doi:10.1088/1126-6708/2009/04/003, arXiv:0811.3458.

[40] D. de Florian and M. Grazzini, "Higgs production through gluon fusion: updated cross sections at the Tevatron and the LHC", *Phys. Lett. B* **674** (2009) 291–294, doi:10.1016/j.physletb.2009.03.033, arXiv:0901.2427.

[41] Baglio, J. and Djouadi, A., "Higgs production at the LHC", *JHEP* **03** (2011) 055, doi:10.1007/JHEP03(2011)055, arXiv:1012.0530.

[42] D. de Florian and M. Grazzini, "Higgs production at the LHC: updated cross sections at $\sqrt{s} = 8$ TeV", arXiv:1206.4133.

[43] G. Bozzi et al., "Transverse-momentum resummation and the spectrum of the Higgs boson at the LHC", *Nucl. Phys. B* **737** (2006) 73–120, doi:10.1016/j.nuclphysb.2005.12.022, arXiv:hep-ph/0508068.

[44] D. de Florian et al., "Transverse-momentum resummation: Higgs boson production at the Tevatron and the LHC", *JHEP* **11** (2011) 064, doi:10.1007/JHEP11(2011)064.

[45] G. Passarino, C. Sturm, and S. Uccirati, "Higgs Pseudo-Observables, Second Riemann Sheet and All That", *Nucl. Phys. B* **834** (2010) 77–115, doi:10.1016/j.nuclphysb.2010.03.013, arXiv:1001.3360.

[46] I. W. Stewart and F. J. Tackmann, "Theory Uncertainties for Higgs and Other Searches Using Jet Bins", (2011). arXiv:1107.2117.

[47] A. Djouadi, J. Kalinowski, and M. Spira, "HDECAY: A program for Higgs boson decays in the standard model and its supersymmetric extension", *Comput. Phys. Commun.* **108** (1998) 56–74, doi:10.1016/S0010-4655(97)00123-9, arXiv:hep-ph/9704448.

[48] A. Djouadi et al., "An update of the program HDECAY", in *The Les Houches 2009 workshop on TeV colliders: The tools and Monte Carlo working group summary report*. 2010. arXiv:1003.1643.

[49] A. Bredenstein et al., "Precise predictions for the Higgs-boson decay H $\to$ WW/ZZ $\to$ 4 leptons", *Phys. Rev. D* **74** (2006) 013004, doi:10.1103/PhysRevD.74.013004, arXiv:hep-ph/0604011.

[50] A. Bredenstein et al., "Radiative corrections to the semileptonic and hadronic Higgs-boson decays H $\to$W W / Z Z$\to$ 4 fermions", *JHEP* **0702** (2007) 080, doi:10.1088/1126-6708/2007/02/080, arXiv:hep-ph/0611234.

[51] S. Actis et al., "NNLO Computational Techniques: the Cases $H \to \gamma\gamma$ and $H \to gg$", *Nucl. Phys. B* **811** (2009) 182–273, doi:10.1016/j.nuclphysb.2008.11.024, arXiv:0809.3667.

[52] A. Denner et al., "Standard Model Higgs-Boson Branching Ratios with Uncertainties", *Eur. Phys. J. C* **71** (2011) 1753, doi:10.1140/epjc/s10052-011-1753-8, arXiv:1107.5909.

[53] M. Ciccolini et al., "Strong and electroweak corrections to the production of Higgs + 2-jets via weak interactions at the LHC", *Phys. Rev. Lett.* **99** (2007) 161803, doi:10.1103/PhysRevLett.99.161803, arXiv:0707.0381.

[54] M. Ciccolini at al., "Electroweak and QCD corrections to Higgs production via vector-boson fusion at the LHC", *Phys. Rev. D* **77** (2008) 013002, doi:10.1103/PhysRevD.77.013002, arXiv:0710.4749.

[55] T. Figy, C. Oleari, and D. Zeppenfeld, "Next-to-leading order jet distributions for Higgs boson production via weak-boson fusion", *Phys. Rev. D* **68** (2003) 073005, doi:10.1103/PhysRevD.68.073005, arXiv:hep-ph/0306109.

[56] K. Arnold et al., "VBFNLO: A parton level Monte Carlo for processes with electroweak bosons", *Comput. Phys. Commun.* **180** (2009) 1661–1670, doi:10.1016/j.cpc.2009.03.006, arXiv:0811.4559.

[57] P. Bolzoni et al., "Higgs production via vector-boson fusion at NNLO in QC D", *Phys. Rev. Lett.* **105** (2010) 011801, doi:10.1103/PhysRevLett.105.011801, arXiv:1003.4451.

[58] T. Han and S. Willenbrock, "QCD correction to the $pp \to WH$ and ZH total cross-sections", *Phys. Lett. B* **273** (1991) 167–172, doi:10.1016/0370-2693(91)90572-8.

[59] O. Brein, A. Djouadi, and R. Harlander, "NNLO QCD corrections to the Higgs-strahlung processes at hadron colliders", *Phys. Lett. B* **579** (2004) 149–156, doi:10.1016/j.physletb.2003.10.112, arXiv:hep-ph/0307206.

[60] M. L. Ciccolini, S. Dittmaier, and M. Krämer, "Electroweak radiative corrections to associated WH and ZH production at hadron colliders", *Phys. Rev. D* **68** (2003) 073003, doi:10.1103/PhysRevD.68.073003, arXiv:hep-ph/0306234.

[61] R. Hamberg, W. L. van Neerven, and T. Matsuura, "A complete calculation of the order α_S^2 correction to the Drell-Yan K factor", *Nucl. Phys. B* **359** (1991) 343–405, doi:10.1016/0550-3213(91)90064-5.

[62] A. Denner et al., "EW corrections to Higgs strahlung at the Tevatron and the LHC with HAWK", (2011). arXiv:1112.5258.

[63] G. Ferrera, M. Grazzini, and F. Tramontano, "Associated WH production at hadron colliders: a fully exclusive QCD calculation at NNLO", *Phys. Rev. Lett.* **107** (2011) 152003, doi:10.1103/PhysRevLett.107.152003, arXiv:1107.1164.

[64] W. Beenakker et al., "Higgs radiation off top quarks at the Tevatron and the LHC", *Phys. Rev. Lett.* **87** (2001) 201805, doi:10.1103/PhysRevLett.87.201805, arXiv:hep-ph/0107081.

[65] W. Beenakker et al., "NLO QCD corrections to $t\bar{t}$ H production in hadron collisions.", *Nucl. Phys. B* **653** (2003) 151–203, doi:10.1016/S0550-3213(03)00044-0, arXiv:hep-ph/0211352.

[66] S. Dawson et al. , "Associated top quark Higgs boson production at the LHC", *Phys. Rev. D* **67** (2003) 071503, doi:10.1103/PhysRevD.67.071503, arXiv:hep-ph/0211438.

[67] S. Dawson et al., "Associated Higgs production with top quarks at the Large Hadron Collider: NLO QCD corrections", *Phys. Rev. D* **68** (2003) 034022, doi:10.1103/PhysRevD.68.034022, arXiv:hep-ph/0305087.

[68] M. Botje et al., "The PDF4LHC Working Group Interim Recommendations", (2011). arXiv:1101.0538.

[69] S. Alekhin et al., "The PDF4LHC Working Group Interim Report", (2011). arXiv:1101.0536.

[70] H.-L. Lai et al., "New parton distributions for collider physics", *Phys. Rev. D* **82** (2010) 074024, doi:10.1103/PhysRevD.82.074024, arXiv:1007.2241.

[71] A.D. Martin et al., "Parton distributions for the LHC", *Eur. Phys. J. C* **63** (2009) 189–285, doi:10.1140/epjc/s10052-009-1072-5, arXiv:0901.0002.

[72] NNPDF Collaboration, "Impact of Heavy Quark Masses on Parton Distributions and LHC Phenomenology", *Nucl. Phys. B* **849** (2011) doi:10.1016/j.nuclphysb.2011.03.021, arXiv:1101.1300.

[73] CMS Collaboration, "Evidence for a new state decaying into two photons in the search for the standard model Higgs boson in pp collisions", *CMS Physics Analysis Summary* **CMS-PAS-HIG-12-015** (2012).

[74] CMS Collaboration, "Search for the standard model Higgs boson produced in association withW or Z bosons, and decaying to bottom quarks", *CMS Physics Analysis Summary* **CMS-PAS-HIG-12-019** (2012).

[75] CMS Collaboration, "Search for Higgs production in association with top quark pairs in pp collisions", *CMS Physics Analysis Summary* **CMS-PAS-HIG-12-025** (2012).

[76] CMS Collaboration, "Search for neutral Higgs bosons decaying to tau pairs in pp collisions", *CMS Physics Analysis Summary* **CMS-PAS-HIG-12-018** (2012).

[77] CMS Collaboration, "Search for the standard model Higgs boson decaying into $\tau\tau$ and WW associated with Z", *CMS Physics Analysis Summary* **CMS-PAS-HIG-12-012** (2012).

[78] CMS Collaboration, "Search for the standard model Higgs boson in associated WH production in the $e\mu\tau$ and $\mu\mu\tau$ final states", *CMS Physics Analysis Summary* **CMS-PAS-HIG-12-006** (2012).

[79] CMS Collaboration, "Search for the Standard Model Higgs boson in the $H \to WW \to lvjj$ decay channel", *CMS Physics Analysis Summary* **CMS-PAS-HIG-12-003** (2012).

[80] CMS Collaboration, "Search for the Standard Model Higgs boson in the $H \to WW \to lvjj$ decay channel in pp collisions at $\sqrt{s}$ = 8 TeV", *CMS Physics Analysis Summary* **CMS-PAS-HIG-12-021** (2012).

[81] CMS Collaboration, "Search for the Higgs Boson Decaying to W^+W^- in the Fully Leptonic Final State", *CMS Physics Analysis Summary* **CMS-PAS-HIG-11-024** (2011).

[82] CMS Collaboration, "Search for the standard model Higgs boson decaying to W^+W^- in the fully leptonic final state in pp collisions at $\sqrt{s}$ = 8 TeV", *CMS Physics Analysis Summary* **CMS-PAS-HIG-12-017** (2012).

[83] CMS Collaboration, "Study of associated Higgs boson (WH) Production in the three leptons final state at 7 TeV", *CMS Physics Analysis Summary* **CMS-PAS-HIG-11-034** (2011).

[84] CMS Collaboration, "Search for associated Higgs production (VH) with $H \to W^+W^- \to lvlv$ and hadronic V decay in pp collisions at $\sqrt{s}$ = 7 TeV", *CMS Physics Analysis Summary* **CMS-PAS-HIG-12-014** (2012).

[85] CMS Collaboration, "Evidence for a new state in the search for the standard model Higgs boson in the $H \to ZZ \to 4l$ channel in pp collisions at $\sqrt{s}$ = 7 and 8 TeV", *CMS Physics Analysis Summary* **CMS-PAS-HIG-12-016** (2012).

[86] CMS Collaboration, "Search for a Higgs boson in the decay channel $H \to ZZ \to 2lqq$", *CMS Physics Analysis Summary* **CMS-PAS-HIG-11-027** (2011).

[87] CMS Collaboration, "Search for the standard model Higgs boson in the $H \to ZZ \to 2l2\nu$ channel in pp collisions at $\sqrt{s}$ = 7 and 8 TeV", *CMS Physics Analysis Summary* **CMS-PAS-HIG-12-023** (2012).

[88] CMS Collaboration, "Algorithms for b jet identification in CMS", (2009). CMS Physics Analysis Summary CMS-PAS-BTV-09-001.

[89] ATLAS and CMS Collaborations, LHC Higgs Combination Group, "Procedure for the LHC Higgs boson search combination in Summer 2011", Technical Report ATL-PHYS-PUB 2011-11, CMS NOTE 2011/005, (2011). http://cdsweb.cern.ch/record/1379837.

[90] G. Cowan et al., "Asymptotic formulae for likelihood-based tests of new physics", *Eur. Phys. J. C* **71** (2011) 1–19, doi:10.1140/epjc/s10052-011-1554-0, arXiv:1007.1727.

[91] Moneta, L. et al., "The RooStats Project", in *13th International Workshop on Advanced Computing and Analysis Techniques in Physics Research (ACAT2010)*. SISSA, 2010. arXiv:1009.1003. PoS(ACAT2010)057.

[92] T. Junk, "Confidence level computation for combining searches with small statistics", *Nucl. Instrum. Meth. A* **434** (1999) 435–443, doi:10.1016/S0168-9002(99)00498-2.

[93] A. L. Read, "Presentation of search results: the CLs technique", *J. Phys. G: Nucl. Part. Phys.* **28** (2002) 2693, doi:10.1088/0954-3899/28/10/313.

[94] Gross, E. and Vitells, O., "Trial factors for the look elsewhere effect in high energy physics", *Eur. Phys. J. C* **70** (2010) 525–530, doi:10.1140/epjc/s10052-010-1470-8, arXiv:1005.1891.